Analysis of Fluid Flow Under a Grinding Wheel

M. R. Schumack
Mem. ASME

Jin-Bok Chung

W. W. Schultz
Mem. ASME

E. Kannatey-Asibu, Jr.
Mem. ASME

Department of Mechanical Engineering
and Applied Mechanics,
University of Michigan,
Ann Arbor, MI 48109

Fluid flow under a grinding wheel is modeled using a perturbation scheme. In this initial effort to understand the flow characteristics, we concentrate on the case of a smooth wheel with slight clearance between the wheel and workpiece. The solution at lowest order is that given by standard lubrication theory. Higher-order terms correct for inertial and two-dimensional effects. Experimental and analytical pressure profiles are compared to test the validity of the model. Lubrication theory provides good agreement with low Reynolds number flows; the perturbation scheme provides reasonable agreement with moderate Reynolds number flows but fails at high Reynolds numbers. Results from experiments demonstrate that the ignored upstream and downstream conditions significantly affect the flow characteristics, implying that only a model based on the fully two- (or three-) dimensional Navier-Stokes equations will accurately predict the flow. We make one comparison between an experiment with a grinding wheel and the model incorporating a one-dimensional sinusoidal roughness term. For this case, lubrication theory surprisingly provides good agreement with experiment.

1 Introduction

Application of fluid to the region between a grinding wheel and workpiece serves four principal purposes: cooling, lubrication, removal of worked particles, and chemical protection of the work-piece surface. Studies have only touched upon aspects of the flow mechanisms under a grinding wheel; no one has yet developed a comprehensive flow model. Hahn [8] discusses how the lubrication equation applies to the tiny clearances between the grit and work surface. Andrew [1] presents a model developed by Powell [13] that describes the fluid flow through a porous wheel when applied by a shoe. Others have presented roughness models for lubrication flows [10, 11, 17]. The phenomenon of "starved" lubrication flow has been investigated by Constantinescu [3] and Lauder [9].

In this paper, we restrict our analysis to bulk fluid behavior and do not model the local lubrication phenomenon at the grinding wheel grains. We apply the basic lubrication equation (Reynold's equation) with appropriate modifications to analyze the fluid flow and pressure distribution under conditions similar to surface grinding. We concentrate on a two-dimensional formulation where we neglect flow in the z-direction (in the direction of the wheel width, Fig. 1). Most derivations of the lubrication equation assume that fluid inertia, pressure gradients across the fluid film, and velocity gradients other than those across the fluid film can be neglected and that the fluid is incompressible. Due to the high wheel speeds in the grinding process, the assumption of no inertial effects may be invalid. Therefore, in our analysis, we introduce a scaling into the incompressible two-dimensional Navier-Stokes equations that allows calculation of inertial and two-dimensional corrections to the lubrication equation. Mitsuya [10] developed a perturbation solution including two-dimensional viscous effects, but neglected inertial terms. Reinhardt's [14] perturbation scheme included small inertial terms but neglected two-dimensional viscous effects and the entire y-component of the Navier-Stokes equations. Our perturbation scheme includes both inertial and two-dimensional effects from both the x- and y-components of the Navier-Stokes equations.

In this initial effort to understand the bulk behavior of grinding fluid flow, we concentrate on flow under a smooth wheel with a small clearance between the wheel and workpiece. We do, however, add a sinusoidal roughness to the model for comparison with a grinding wheel experiment (see section 4). Although viscosity can be affected by the large amount of heat generated during actual grinding, we ignore temperature effects in this analysis because no significant contact occurs between the wheel and workpiece in our experiments. Pressure is small in grinding situations and hence does not influence the viscosity.

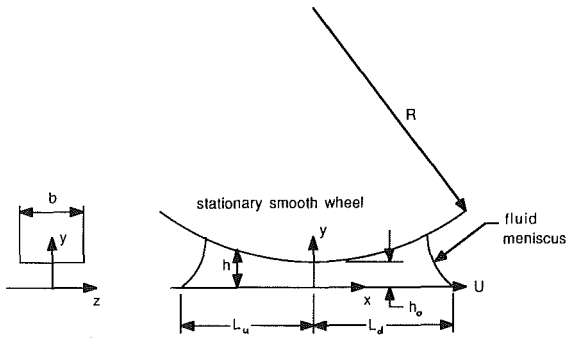

Fig. 1 Model geometry

Contributed by the Production Engineering Division for publication in the JOURNAL OF ENGINEERING FOR INDUSTRY. Manuscript received July 1989; revised April 1990.

Although our perturbation scheme leads to calculation of inertial and two-dimensional corrections to the lubrication equation, it cannot account for velocity boundary conditions at the ends of the fluid region where the fluid is injected and where it exits the area under the wheel. In section 3 we present experimental results showing how the flow under the wheel is affected by the end boundary conditions, therefore demonstrating the need for a model based on the full two- (or three-) dimensional Navier-Stokes equations. Finally, in section 4, we make comparisons of pressure profiles from experiments with our perturbation model. Comparisons are made with both smooth and real grinding wheels.

2 Analysis

Flow under a grinding wheel is unsteady because the flow domain changes constantly due to wheel roughness (the workpiece is considered smooth). We usually restrict our analysis to a smooth wheel, which results in a steady flow. However, to incorporate roughness into a steady model, we make the critical assumption that the wheel can be held stationary while the table moves at the peripheral wheel speed. This has the effect of translating the wheel instead of rotating it and greatly simplifies the algebra of the perturbation solution. We have tested this assumption for several of our smooth wheel computations and found it to be quite adequate—the main constraint is that the wheel radius is much larger than the clearance between the wheel and workpiece. (In grinding, the table speed itself is usually much smaller than the wheel peripheral speed and thus can be ignored.) Hence, in our analysis, the constant velocity of the lower surface ($y=0$), U, is the peripheral wheel speed.

We define the fluid flow field region under the wheel in the x-direction using the locations revealed by our experiments, $-L_u \le x \le L_d$, as shown in Fig. 1. These locations are determined from where the gage pressure starts to increase from zero upstream ($x=-L_u$) and where the gage pressure abruptly increases to return to zero downstream ($x=L_d$). The abrupt increase in pressure in the downstream region of the flow has been modeled by Coyne and Elrod [6]; we, however, do not model this rupture phenomenon.

All variables are hereafter presented as dimensionless. The length scales in the x and y directions are the wheel radius R and minimum clearance h_0, respectively. The stream function is scaled on Uh_0.

The two-dimensional stream function form of the dimensionless Navier-Stokes equations for steady, incompressible flow is

$$\epsilon^2 \mathrm{Re}(\psi_y \psi_{xyy} - \psi_x \psi_{yyy}) - \epsilon^4 \mathrm{Re}(\psi_x \psi_{xxy} - \psi_y \psi_{xxx}) = \nabla^4 \psi, \quad (1)$$

where subscripts denote partial differentiation, and

$$\nabla^4 = \frac{\partial^4}{\partial y^4} + 2\epsilon^2 \frac{\partial^4}{\partial x^2 \partial y^2} + \epsilon^4 \frac{\partial^4}{\partial x^4}. \quad (2)$$

The Reynolds number, Re, is defined as $\rho U R/\mu$. The quantity $\epsilon = h_0/R$ is a small parameter to be used in the expansion procedure. This scaling implies that derivatives are small in the horizontal direction as compared to the vertical one. The boundary conditions are

$$\psi = \psi_y - 1 = 0 \text{ at } y=0 \quad (3)$$

and

$$\psi - Q = \psi_y = 0 \text{ at } y=h. \quad (4)$$

The parameter $Q = \int_0^h u\, dy$ is the dimensionless volumetric flow rate per unit wheel width, scaled on Uh_0. Later we describe how we determine Q iteratively.

The solution procedure will not allow arbitrary velocity boundary conditions at $x=L_d$ and $x=-L_u$ since we have scaled the problem as slowly varying in x. The flow near the two menisci are two-dimensional boundary corrections and must be solved by a fully computational method [4, 15]. We do not know the end boundary conditions; thus we assume that the expansion solution is valid everywhere. Since ϵ appears in the equations of motion in even powers, we expand the stream function as

$$\psi = \psi_0 + \epsilon^2 \psi_2 + \epsilon^4 \psi_4 + \ldots$$

The slowly varying expansion succeeds since the scaling requires that the boundary conditions (3) and (4) be applied as if h is nearly a constant. Variations from the standard parabolic velocity profile caused by larger variations in h then come in at higher orders. The equation at order unity becomes

$$\psi_{0_{yyyy}} = 0, \quad (5)$$

with the boundary conditions

$$\psi_0 = \psi_{0_y} - 1 = 0 \text{ at } y=0 \quad (6)$$

and

$$\psi_0 - Q = \psi_{0_y} = 0 \text{ at } y=h. \quad (7)$$

The solution to (5) is simply

$$\psi_0 = A + By + Cy^2 + Dy^3, \quad (8)$$

where A, B, C, and D are functions of z determined by boundary conditions (6) and (7), resulting in

$$\psi_0 = y + y^2\left(\frac{3Q}{h^2} - \frac{2}{h}\right) + y^3\left(\frac{1}{h^2} - \frac{2Q}{h^3}\right). \quad (9)$$

This result to leading order is that given by the one-

Nomenclature

p = pressure, nondimensionalized with $\mu UR/h_0^2$
h_0 = minimum clearance under the wheel
μ = absolute viscosity
ρ = density
ν = kinematic viscosity
U = circumferential wheel speed
R = wheel radius
x = coordinate axis in horizontal direction, nondimensionalized with R
y = coordinate axis in vertical direction, nondimensionalized with h_0
z = coordinate axis in direction of wheel width, nondimensionalized with R
h = height of wheel above workpiece, nondimensionalized with h_0
Q = flow rate per unit wheel width, nondimensionalized with Uh_0, model input
Q^* = experimentally measured flow rate under the wheel at $x=0$
ψ = stream function, nondimensionalized with Uh_0
Re = Reynolds number, $\rho UR/\mu$
Re_∞ = Reynolds number as defined in [7] and [18]
ϵ = slenderness ratio h_0/R
L = length of fluid region under wheel from meniscus to wheel center, nondimensionalized with R.
u = velocity in x-direction, nondimensionalized with U
b = wheel width

Subscripts

x, y = differentiation with respect to
0, 2, 4 = order of solution
u = upstream
d = downstream

dimensional lubrication equation. At the next order, $O(\epsilon^2)$, the equation becomes

$$\psi_{2_{yyyy}} = -2\psi_{0_{xxyy}} + \mathrm{Re}(\psi_{0_y}\psi_{0_{xyy}} - \psi_{0_x}\psi_{0_{yyy}}) \tag{10}$$

with the boundary conditions

$$\psi_2 = \psi_{2_y} = 0 \text{ at } y = 0 \tag{11}$$

and

$$\psi_2 = \psi_{2_y} = 0 \text{ at } y = h. \tag{12}$$

The solution to (10) through (12) given by the symbolic manipulator REDUCE is

$$\begin{aligned}\psi_2 = \mathrm{Re}\ & h'y^2[1/14(Q/h) - 1/42(y/h) - 3/35(Q/h)^2 \\ & - 1/70(Qy/h^2) + 1/6(y^2/h^2) + 9/35(Q^2y/h^3) \\ & - 1/2(Qy^2/h^3) - 7/30(y^3/h^3) + 9/10(Qy^3/h^4) \\ & + 2/15(y^4/h^4) - 3/5(Q^2y^3/h^5) - 3/5(Qy^4/h^5) \\ & - 1/35(y^5/h^5) + 3/5(Q^2y^4/h^6) + 1/7(Qy^5/h^6) \\ & - 6/35(Q^2y^5/h^7) - 1/70] + y^2[-1/5(Qh''/h) \\ & + 1/15(h''y/h) - 1/5(h''Qy/h^2) - 1/3(y^2h''/h^2) \\ & + Qy^2h''/h^3 + 1/5(h''y^3/h^3) - 3/5(Qy^3h''/h^4) \\ & + 1/15(h'') - 8/15(h'^2/h) + 9/5(Qh'^2/h^2) \\ & + 7/15(h'^2y/h^2) - 6/5(Qyh'^2/h^3) + 2/3(y^2h'^2/h^3) \\ & - 3Qy^2h'^2/h^4 - 3/5(y^3h'^2/h^4) + 12/5(Qy^3h'^2/h^5)].\end{aligned} \tag{13}$$

Here, the prime indicates differentiation with respect to x. This correction shows the first effects of inertia and two-dimensional viscous forces. The pressure can be determined by examining the scaled Stokes equations to order ϵ^2:

$$p_x = \psi_{yyy} + \epsilon^2\psi_{xxy} - \epsilon^2\ \mathrm{Re}(\psi_y\psi_{xy} - \psi_x\psi_{yy}) \tag{14}$$

and

$$p_y = -\epsilon^2\psi_{xyy} + O(\epsilon^4). \tag{15}$$

The pressure scale is $\mu UR/h_0^2$. Expanding pressure in the even power series, substituting (9) and (13) into (14) and (15), and integrating gives the standard lubrication equation at lowest order:

$$p_0 = 6\int \frac{1}{h^2}\,dx - 2Q\int \frac{1}{h^3}\,dx, \tag{16}$$

where the constant of integration is chosen so that $p(x = -L_u) = 0$. The next order shows dependence on the Reynolds number and y as well:

$$\begin{aligned}p_2 = \mathrm{Re}[& -27/35(Q^2/h^2) + 3/35(Q/h) - 1/7\ \ln(h)] \\ & + 2/5(h'/h) - 6/5(h'Q/h^2) - 4yh'/h^2 \\ & + 12Qyh'/h^3 + 6y^2h'/h^3 - 18Qy^2h'/h^4 \\ & - 48/5\left(Q\int h'^2/h^3dx\right) + 16/5\left(\int h'^2/h^2dx\right).\end{aligned} \tag{17}$$

Two parameters are unknown, Q and the upstream position L_u where the pressure begins to rise from ambient. Others have suggested methods for determining these parameters for a "starved" lubrication flow (upstream [9] and downstream [6]). We do not formally apply the above pressure boundary conditions, but instead we manipulate the values for Q and L_u until reasonable agreement with experiments is obtained. If suitable values of Q and L_u cannot be found, we conclude that the model fails. As will be seen, our perturbation solution (16) and (17) describes low and moderate Reynolds number flows well, but cannot accurately predict higher Reynolds number flows regardless of the chosen values for Q and L_u.

The results obtained from the perturbation technique are identical to those presented in Mitsuya [10] in the limit of zero Reynolds number. Our analysis indicates that the Reynolds number effects at $O(\epsilon^2)$ are more important than the two-dimensional noninertial effects. Therefore, we will compare our method with a model where inertia effects are added less formally [14, 18] (see section 4). Rather than using numerical integration of (16) and (17), the pressure profiles are obtained by the equivalent procedure using a Runge-Kutta-Fehlberg technique to integrate (14) using exact expressions for height. To determine the effect of wheel roughness, we add a sinusoidal term of the form $A\cos(\omega x)$ to the smooth wheel height expression (see section 4).

A different form of the standard lubrication equation accounting for circumferential and axial flows under the wheel (flow in x and z directions) is given by [12, 16]

$$\frac{\partial}{\partial x}(h^3\partial p/\partial x) + \frac{\partial}{\partial z}(h^3\partial p/\partial z) = 6\frac{\partial h}{\partial x}. \tag{18}$$

Here, z is scaled on the radius R. This form of the lubrication equation models side leakage from under the wheel. Equation (18) was solved using finite differences, with $p = 0$ at $x = -L_u$ and L_d and $z = \pm(b/R)/2$, where b is the wheel width. The results for the pressure along the wheel centerline ($z = 0$) are nearly identical to those for the lubrication equation ignoring axial flow (16) and add nothing new to our understanding of grinding flows. Therefore, in section 4 we present only the results from (14).

3 Experiments

We designed experiments to test the influence of end boundary conditions (at $x = L_u$, L_d) and to verify the preceding analysis. Data were obtained mainly for a smooth wheel on a surface grinder with low clearance between the wheel and workpiece. Some data, however, were obtained with grinding wheels to determine the effect of surface roughness. Three wheel types were used: a relatively fine-grain grinding wheel (SA120M10V3W), a relatively rough-grain grinding wheel (23A60), and a smooth plastic wheel. The fine-grain wheel was 349 mm diameter and 25.4 mm wide, the rough-grain wheel was 356 mm diameter and 25.4 mm wide, and the smooth wheel was 318 mm diameter and 23.8 mm wide.

The varied parameters included the nozzle position, nozzle jet velocity, nozzle volumetric flow rate, type of grinding fluid, and type of wheel (smooth or grinding). Measured parameters were the fluid pressure and volumetric fluid flow rate under the wheel.

A reciprocating table grinder with variable speed was used for the experiments. All measured signals were first sampled using a 12-bit data acquisition system and stored on a personal computer for subsequent analysis.

The grinding fluids included water, oil/water mixtures, pure oil, and a detergent/water mixture. The oil/water mixtures had viscosities approximately equal to water. The pure oil (Chrysan Industries type G7-2) had a viscosity of approximately 70 times that of water as measured with a Brookfield Couette viscometer.

Pressure measurements were made using a pressure transducer inserted beneath a hole drilled in the workpiece (Fig. 2). The effect of hole size on the measured pressure was investigated using two different hole diameters, 0.79 mm and 2.38 mm. Table 1 shows that the maximum values from the pressure profile differed only slightly for the two hole diameters. The larger hole resulted in lower negative pressures, possibly due to more recirculation in the larger cavity. However, hole diameter made little difference on positive pressure readings. We used a 2.38 mm diameter hole for the remaining measurements presented here.

Tests showed that strains applied to the workpiece did not influence the pressure readings by distorting the transducer but vibrations added significantly to the pressure signal noise.

Table 1 Pressure vs. hole diameter (smooth wheel), small clearance, water as grinding fluid, 1900 rpm, pressures accurate to ±1 kPa

HOLE DIA. (mm)	MAX. PRESS. (kPa, gauge)	MIN. PRESS. (kPa, gauge)
2.38	12.20	-6.00
.79	12.34	-2.27

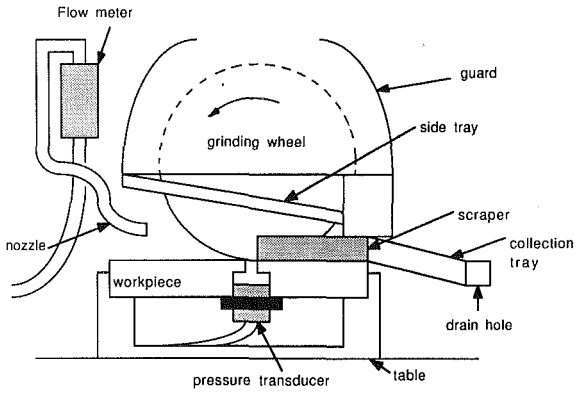

Fig. 2 Experimental set-up

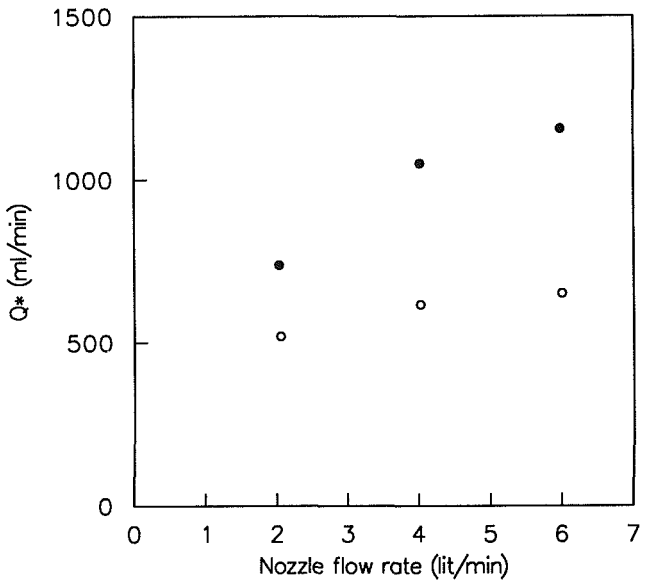

Fig. 3 Q* vs. nozzle flow rate for different heights, smooth wheel, 1920 rpm, 5 percent oil/water mix, high nozzle position, ○ .025 mm ● .076 mm

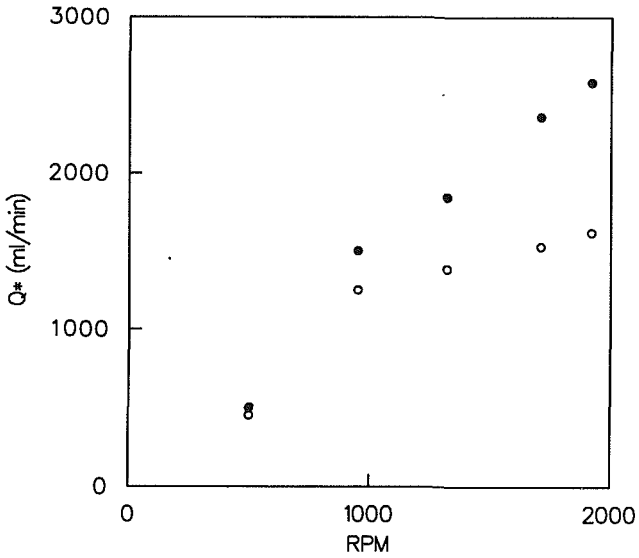

Fig. 4 Q* vs. wheel rpm for varying nozzle flow rate, fine-grain grinding wheel, jet velocity = 3.54 m/s, water, high nozzle position, ○ 2 l/min ● 4.1 l/min

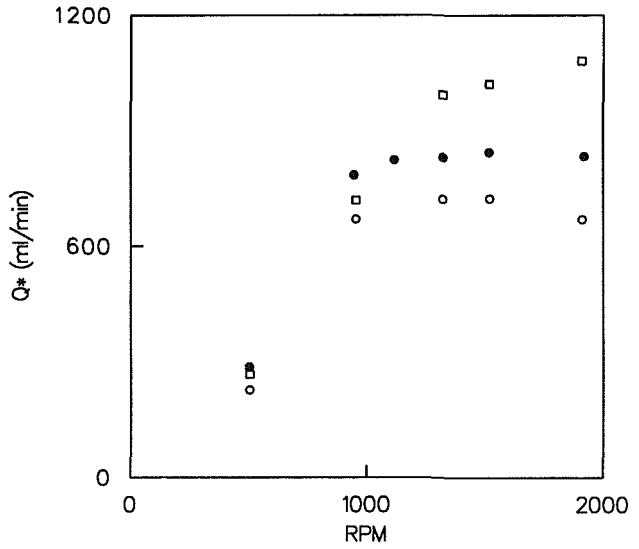

Fig. 5 Q* vs. wheel rpm for varying jet velocity, smooth wheel, nozzle flow rate = 3.5 l/min, 1 percent oil/water mix, low nozzle position, height = .076 mm, ○ 1.55 m/s ● 3.02 m/s □ 6.03 m/s

The pressure data was not filtered other than that in the digitization process.

A table position indicator with its base fastened to the moving table and an arm connected to the stationary wheel housing indicated when the pressure tap passed under the grinding wheel, to within 2 mm. An electric circuit was broken when the pressure tap passed under the wheel centerline; the circuit was completed 25 mm beyond the wheel centerline, allowing determination of both the location of wheel centerline ($x=0$) and the average table speed.

Flow rate under the wheel at $x=0$—denoted as Q^*—was measured using the collection tray illustrated in Fig. 2. A side tray collected fluid flung off the wheel against the wheel guard; this flow was included in Q^*. A scraper along the side of the wheel flush with the workpiece surface ensured that any fluid leaving the area under the wheel prior to the wheel centerline ($x=0$) was not added to Q^*. The collection system ensured that nearly all flow traveling under the wheel at $x=0$ was measured.

It was difficult to quantify the minimum clearance between the wheel and the workpiece due to irregularities of the wheels and inaccuracies in the height adjustment mechanism of the grinder. Centrifugal forces also "stretched" the plastic wheel slightly (≈ .025 mm) during high-speed operation. In addition, discrepancies existed between the height indicated by the height controller of the grinder and as needed in the model to achieve reasonable agreement with experimental pressure profiles. For instance, in one case the height controller read 0.025 mm while an input of $h_0 = 0.15$ mm was necessary to provide reasonable agreement with the experimental pressure profile. All of the experiments with the grinding wheels (except for those involving pressure measurements) were done under flush grinding conditions, i.e., at a height where the wheel just sparked against the workpiece surface.

Error Analysis for Flow Rate and Pressure Measurements. For measurements of flow rate under the wheel, we estimate an accuracy of ±150 ml/min for the smooth wheel and ±250 ml/min for the grinding wheel. There was greater inconsistency at low speed than at high speed for both wheels: at low

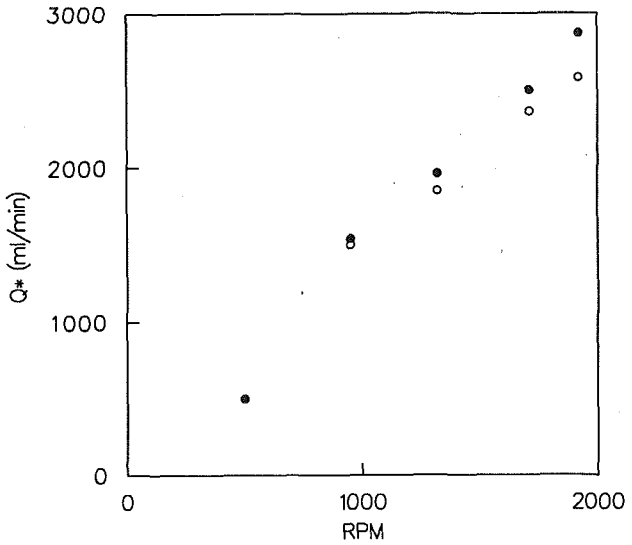

Fig. 6 Q^* vs. wheel rpm for varying jet velocity, fine-grain grinding wheel, nozzle flow rate = 4.1 l/min, water, high nozzle position, • 6.03 m/s ○ 3.02 m/s

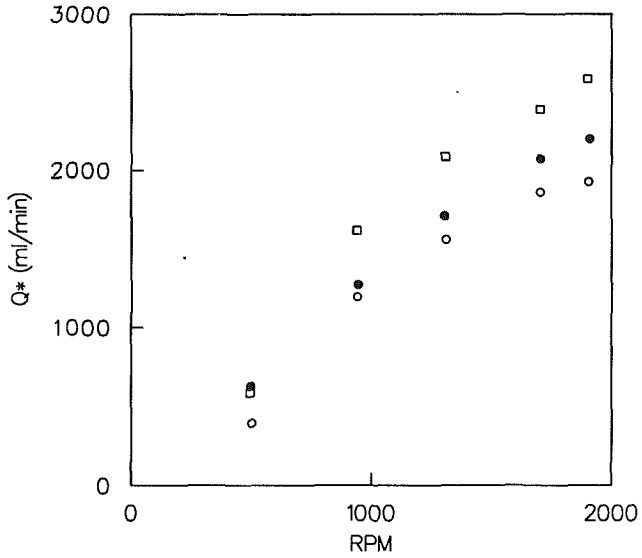

Fig. 8 Q^* vs. wheel rpm for varying nozzle position, fine-grain grinding wheel, nozzle flow rate = 3.5 l/min, jet velocity = 6.03 m/s, water, ○ low nozzle position, • medium nozzle position □ high nozzle position

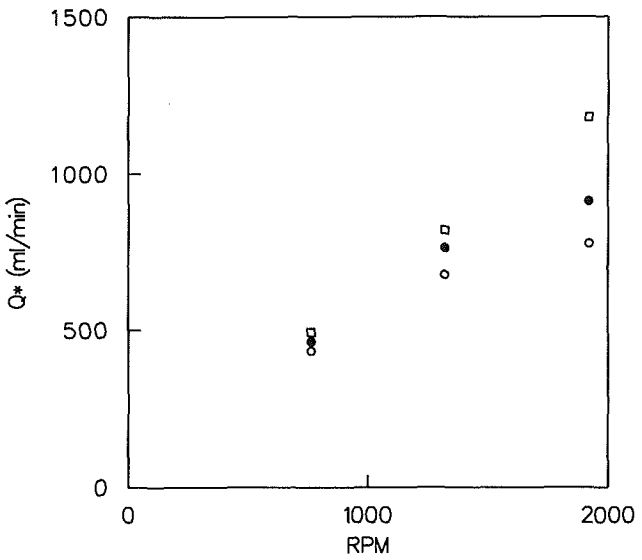

Fig. 7 Q^* vs. wheel rpm for varying nozzle position, smooth wheel, nozzle flow rate = 2.5 l/min, jet velocity = 4.14 m/s, 10 percent oil/water mix, height = .076 mm, ○ low nozzle position • medium nozzle position □ high nozzle position

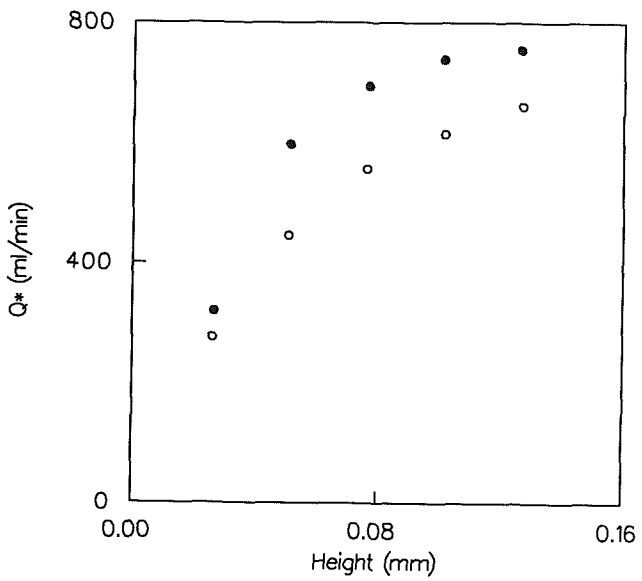

Fig. 9 Q^* vs. height for water and detergent/water mix, smooth wheel, 1920 rpm, nozzle flow rate = 2.4 l/min, jet velocity = 3.02 m/s, medium nozzle position, • water ○ detergent/water mix

speed, there was an irregular ejection of water from under the wheel, while at high speed, the flow became steady. We estimate an accuracy of ± 1 kPa for pressure measurements.

Nozzle Flow Rate, Nozzle Flow Velocity, and Nozzle Position. For the smooth wheel at the lowest height $h_0 = .025$mm, the nozzle flow rate had negligible effect on Q^*, Fig. 3. However, for the smooth wheel at $h_0 = .076$mm and for the grinding wheel under flush grinding conditions, the nozzle flow rate, nozzle flow velocity, and nozzle position all markedly affected Q^*, Figs. 3 through 8. The "high" nozzle position indicates experiments where the nozzle flow was directed against the wheel edge, the "medium" nozzle position directed the nozzle flow into the gap between the wheel edge and the workpiece surface, and the "low" position directed the nozzle flow mainly against the workpiece surface. The "high' and "low" positions described arcs of approximately +9.5 mm and −9.5 mm, respectively, away from the "medium" position. The figures show that increasing the nozzle flow rate, nozzle jet velocity, and nozzle height all resulted in increased flow under both the smooth and grinding wheels, especially at high wheel speeds. Figure 5, which shows Q^* versus speed for different nozzle jet velocities, also suggests that a critical wheel speed exists beyond which Q^* begins to decrease (this is especially evident for the lowest jet velocity). This may indicate that increased pressure due to inertial effects causes more fluid to escape by the sides rather than passing under the region of minimum clearance.

Surface Tension. Water has more surface tension and less viscosity than oil. In an attempt to isolate the effect of surface tension on flow characteristics, we tested for Q^* with pure water and a 1:75 liquid detergent/water mixture. A detergent/water mixture has less surface tension than pure water, but the viscosity is essentially unaffected. As seen in Fig. 9, pure water resulted in 18 percent to 35 percent higher Q^*, especially at higher clearances. The differences between pure water and a detergent/water mixture with a grinding wheel under flush grinding conditions was negligible (Fig. 10).

The experimental results show that inlet conditions in the form of flow rates, flow entry angle, and surface tension all

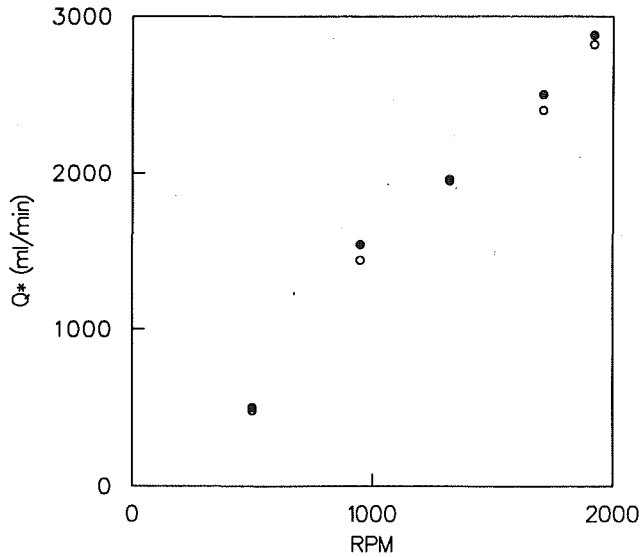

Fig. 10 Q* vs. wheel rpm for water and detergent/water mix, fine-grain grinding wheel, nozzle flow rate = 4.1 l/min, jet velocity = 7.07 m/s, high nozzle position, • water ○ detergent/water mix

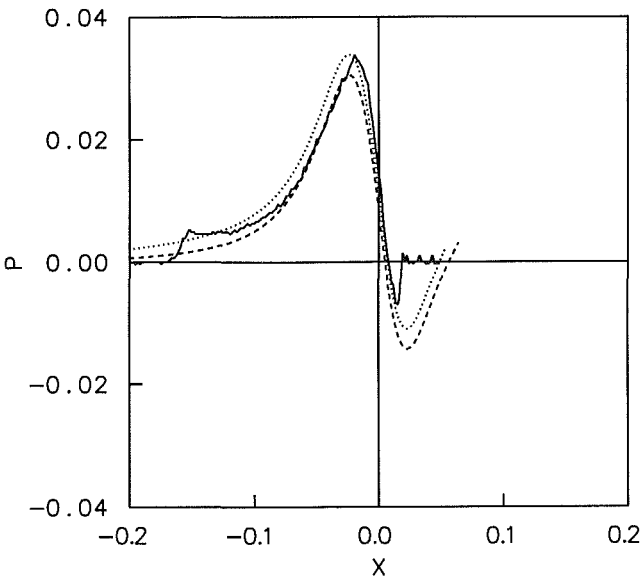

Fig. 11 Comparison of pressure profile for model and experiment, oil ($\mu = .0627$ N·s/m^2, $\rho = 852$ kg/m^3), smooth wheel, 220 rpm, Re = 7800, height = .152 mm, $\epsilon = .00096$, $Q = .64$. Solid line: experiment, $L_u = .17$. Dashed line: lubrication theory, $L_u = .4$. Dotted line: lubrication theory plus corrections, $L_u = .4$

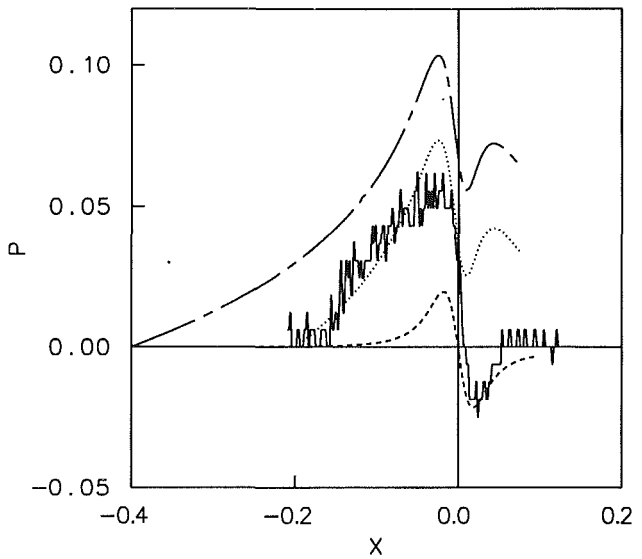

Fig. 12 Comparison of pressure profile for model and experiment, water ($\mu = .000896$ N·s/m^2), smooth wheel, 220 rpm, Re = 6.45 × 10^5, height = .076 mm, $\epsilon = .00048$, $Q = .67$. Solid line: experiment, $L_u = .15$. Dashed line: lubrication theory, $L_u = .4$. Chain-dashed line: lubrication theory plus corrections, $L_u = .4$. Dotted line: lubrication theory plus corrections, $L_u = .2$

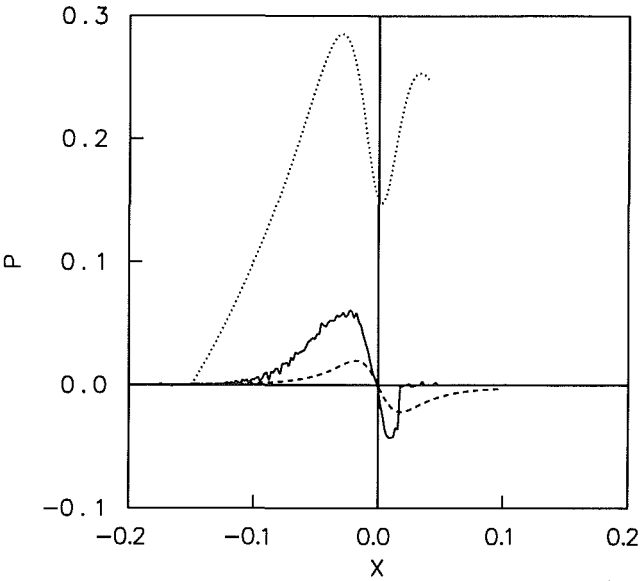

Fig. 13 Comparison of pressure profile for model and experiment, water, smooth wheel, 1339 rpm, Re = 3.9 × 10^6, height = .076 mm, $\epsilon = .00048$, $Q = .67$. Solid line: experiment, $L_u = .12$. Dashed line: lubrication theory, $L_u = .4$. Dotted line: lubrication theory plus corrections, $L_u = .15$

affect the amount of fluid traveling under the wheel and presumably other flow variables such as pressure and velocities. Our perturbation model does not incorporate these boundary conditions, hence the experiments discussed above emphasize the inadequacy of our analysis and suggest that a two- (or three-) dimensional analysis based on the full Navier-Stokes equations is needed.

4 Comparison of Experiment and Analysis

We present comparisons of analytical and experimental pressure profiles for low, moderate, and high Reynolds number flows. As mentioned in section 2, our model does not account for the film rupture phenomenon in the downstream (diverging) part of the flow; the following comparisons therefore concentrate on the upstream (converging) part of the flow.

Figure 11 shows low Re flow ($\epsilon^2 \mathrm{Re} = .007$) using oil. The corrections in the perturbation expansion are small for this flow, and lubrication theory does a good job of modeling the pressure profile. Note that the analytical upstream boundary condition is $p = 0$ at $x = -0.4$ (i.e., $L_u = .4$), and would be the appropriate inlet condition for a flooded geometry, because the pressure gradient as given by the Reynold's equation is negligible at this location for the cylinder-plane geometry. The sudden pressure increase in the upstream part of the experimental profile could be due to deceleration of the incoming fluid jet, similar to the phenomenon analyzed by Buckholz [2] for a plane slider bearing.

Figure 12 compares results for a moderate Re ($\epsilon^2 \mathrm{Re} = .15$). The perturbation corrections overpredict the experimental profile, but the corrected solution provides better agreement with experimental results than lubrication theory. If we set the

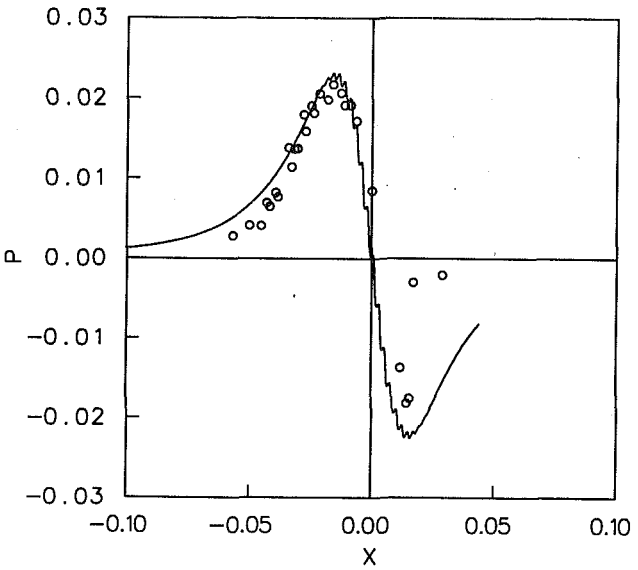

Fig. 14 Comparison of pressure profile for model with roughness and experiment, water, 1154 rpm, $Re = 4.24 \times 10^6$, height = .076 mm, $\epsilon = .00043$, $Q = .575$ ○ experiment, $L_u = .06$. Solid line: lubrication theory with roughness, $L_u = .4$

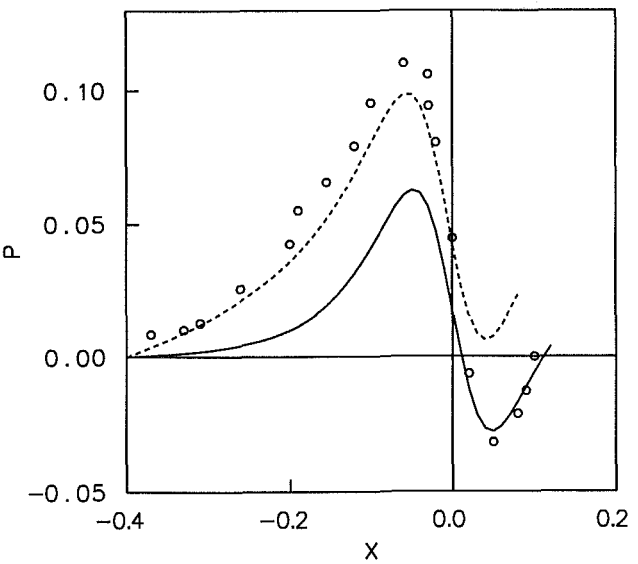

Fig. 15 Comparison of pressure profile for model and Dowson's data, $Re = 7787.5$, $\epsilon^2 Re = .14$, $Re_\infty = 21$, $L_u = .4$, $Q = .636$ (all parameters apply both to Dowson's data and model), ○ Dowson's data. Solid line: lubrication theory. Dashed line: lubrication theory plus corrections

start of the analytical pressure rise closer to that of the experiment (i.e., $p = 0$ at $x \doteq -0.2$), the agreement between the model and experiment becomes quite good.

Figure 13 (corresponding to $\epsilon^2 Re = .9$) demonstrates the failure of the perturbaton model at high Re. The relatively high Reynolds number and low clearance are typical of grinding conditions.

Our analysis reveals that the dominant terms in the second-order correction (17) are those associated with the Reynolds number; the other two-dimensional corrections contribute insignificantly. The parameter ϵ^2 Re is typically used as an indication of the importance of inertial effects in lubrication problems. Note that in the cylinder-plane geometry, this parameter is not solely descriptive of the magnitude of inertial effects. Towards the upstream edge of the lubrication region under the wheel, the pressure correction p_2 increases approximately as Re $\ln(h)$. The parabolic approximation, $h = 1 + x^2/2\epsilon$, shows that for any given x, h increases as ϵ decreases. For grinding-type flows, with moderate-to-high

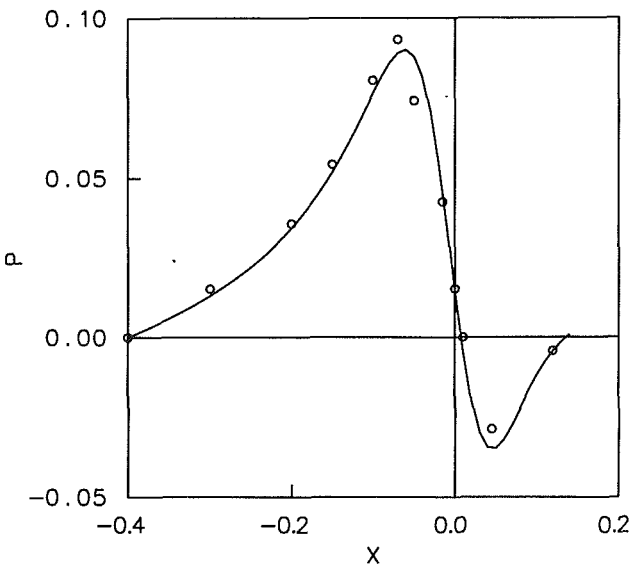

Fig. 16 Comparison of pressure profile for our model and You's model, $Re = 7398.1$, $\epsilon^2 Re = .133$, $Re_\infty = 21$, $L_u = .4$, $Q = .67$ (all parameters apply to both models), ○ You's model. Solid line: our model

Reynolds numbers and small ϵ, the perturbation model fails even though $\epsilon^2 Re \ll 1$.

Figure 14 compares our roughness model results with the pressure profile for a 356 mm diameter rough grain (23A60) grinding wheel at $h_0 = .076$ mm. A roughness frequency of 60 cycles per 25.4 mm and a roughness height of .025 mm correspond to $\omega = 2\pi\ 60R$ and $A = 0.025/h_0$ in the expression $A \cos(\omega x)$ that we add to the equation for the smooth wheel height. The case plotted is a high Re flow (corresponding to $\epsilon^2 Re = .78$). Somewhat unexpectedly, lubrication theory does a good job of modeling the pressure profile. The corrections grossly overpredict the pressure in the same manner as in Fig. 13; we do not plot the corrections here because their exaggerated oscillatory behavior would obscure the experimental and lubrication equation results. As is evident in Figs. 11 through 14, the Reynolds equation gives a relatively narrow pressure profile compared to both the perturbation model and the experiments involving moderate or high Re flows. The high Re experimental profile under the grinding wheel, however, is confined to a relatively narrow region (compare the width of the experimental pressure profiles in Figs. 13 and 14). Perhaps roughness of the grinding wheel results in partial deflection of the incoming coolant jet and a subsequent delay in the beginning of the fully flooded region. This smaller fluid region results in coincidental agreement with lubrication theory.

We have assumed laminar flow in our analysis. Turbulence criteria are lacking for a grinding geometry, but if we apply the criterion for simple two-dimensional Couette flow with no pressure gradient ($Uh/\nu > 1500$) and use h equal to the height at $x = -L_u$, the flow described by Fig. 11 is not turbulent, while the flows described by Figs. 12–14 are turbulent. The same conclusion is reached if we apply the criterion for onset of Taylor vortices (Taylor Number $= Uh/\nu\ (h/R)^{1/2} > 41.3$ [16]). The grinding problem, however, with its complicated boundary condition at the entrance to the flow field offers no simple turbulence criteria.

Figure 15 compares our perturbation model to Dowson's [7] experimental pressure data for a slightly different geometry: a cylinder against a flat plate in a flooded environment. Our perturbation model shows good agreement with the data. Figure 16 compares our perturbation model to that of You [18], who in a perturbation solution from Reinhardt [14] neglected the $\partial^2/\partial x^2$ term in the x-component and the entire y-component of the Navier-Stokes equations. You's equations

incorporated a rupture model for the fluid in the diverging section under the cylinder. Our perturbation model does not account for rupture, but as shown in Fig. 16, good agreement exists between our model and You's in the converging section.

5 Conclusion

For our comparisons involving flow under a smooth wheel, we find that lubrication theory is adequate for describing low Reynolds number flows, but inadequate for describing moderate to high Re flows. Our perturbation model—with two-dimensional and inertial corrections to the lubrication equation—adequately accounts for moderate Reynolds number effects, but not high Re effects. Somewhat surprisingly, and we suspect coincidentally, the Reynolds equation describes the high Re flow under a grinding wheel rather well. We account for this agreement by postulating a reduced flow region under the grinding wheel due to fluid "scatter."

Experiments show that nozzle jet velocity, nozzle angle, volumetric flow rate, and surface tension all affect flow behavior, indicating the significance of conditions at the ends of the fluid flow region. It is also expected that inertial effects would be especially pronounced near the outer regions of the flow field, where the height is much larger than h_0. We conclude that only a model based on the full two- or three-dimensional Navier-Stokes equations incorporating the complex end boundary conditions can adequately model grinding-type flows.

Acknowledgments

This work was funded by General Motors Corporation. We would like to acknowledge the helpful advice of Dr. Chi-Hung Shen and J. C. Lee of GM, and the technical contributions of A. Josephides and W. Courtney while they were students at the University of Michigan. Thanks also to L. Pall in preparation of the manuscript.

References

1 Andrew, C., Howes, T. D., and Pearce, T. R. A., *Creep Feed Grinding*, Holt, Rinehart and Winston, 1985.

2 Buckholz, R. H., "The Effect of Lubricant Inertia Near the Leading Edge of a Plane Slider Bearing," ASME *Journal of Tribology*, Vol. 109, January 1987, pp. 60–64.

3 Constantinescu, Vol. N., "On Some Starvation Phenomena in Fluid Films," *J. Lubr. Tech.*, October 1977, pp. 441–448.

4 Coyle, D. J., Macosko, C. W., and Scriven, L. E., "Film-splitting Flows in Forward Roll Coating," *J. Fluid Mech.*, Vol. 171, 1986, pp. 183–207.

5 Coyne, J. C., and Elrod, H. G., "Conditions for the Rupture of a Lubricating Film, Part I," *J. Lubr. Tech.*, July 1970, pp. 451–456.

6 Coyne, J. C., and Elrod, H. G., "Conditions for the Rupture of a Lubricating Film, Part II," *J. Lubr. Tech.*, January 1971, pp. 156–167.

7 Dowson, D., Smith, E. H., and Taylor, C. M., "An Experimental Study of Hydrodynamic Film Rupture in a Steadily-Loaded, Non-conformal Contact," *J. Mech. Engineering Science*, Vol. 22, 1980, pp. 71–78.

8 Hahn, R. S., "Some Observations on Wear and Lubrication of Grinding Wheels," *Friction and Lubrication in Metal Processing*, F. F. Ling, R. L. Whitely, P. M. Ku, and M. Peterson, eds., ASME, N.Y., 1966.

9 Lauder, W., "Hydrodynamic Lubrication of Proximate Cylindrical Surfaces of Large Relative Curvature," *Proc. Instn. Mech. Engrs.*, Vol. 180, part 3B, 1965, pp. 101–106.

10 Mitsuya, Y., and Fukui, S., "Stokes Roughness Effects on Hydrodynamic Lubrication, Part I-Comparison Between Incompressible and Compresible Lubricating Films," ASME *Journal of Tribology*, Vol. 108, 1986, pp. 151–158.

11 Phan-thien, N., "On the Mean Reynolds Equation in the Presence of Surface Roughness: Squeeze-Film Bearing," ASME *Journal of Applied Mechanics*, Vol. 48, 1981, pp. 717–720.

12 Pinkus, O., and Sternlicht, B., *Theory of Hydrodynamic Lubrication*, McGraw-Hill, 1961.

13 Powell, J. W., "The Application of Grinding Fluid in Creep Feed Grinding," PhD Thesis, University of Bristol, 1979.

14 Reinhardt, E., and Lund, J. W., "The Influence of Fluid Inertia on the Dynamic Properties of Journal Bearings," *J. of Lubrication Technology*, April 1975, pp. 159–165.

15 Ruschak, K. J., "Boundary Conditions at a Liquid/Air Interface in Lubrication Flows," *J. Fluid Mech.*, Vol. 119, 1982, pp. 107–120.

16 Schlichting, H., *Boundary-Layer Theory*, McGraw-Hill, 1979.

17 Shukla, J. B., "A New Theory of Lubrication for Rough Surfaces," *Wear*, Vol. 49, 1978, pp. 33–42.

18 You, H. I., and Lu, S. S., "Inertia Effect in Hydrodynamic Lubrication With Film Rupture," ASME *Journal of Tribology*, Vol. 109, 1987, pp. 86–90.